Localized evaluation of actuator tracking for real-time hybrid simulation using frequency-domain indices

Weijie Xu[1a], Tong Guo[1b] and Cheng Chen[*2]

[1]*Key Laboratory of Concrete and Prestressed Concrete Structures of the Ministry of Education, Southeast University, P.R. China*
[2]*School of Engineering, San Francisco State University, USA*

Abstract. Accurate actuator tracking plays an important role in real-time hybrid simulation (RTHS) to ensure accurate and reliable experimental results. Frequency-domain evaluation index (FEI) interprets actuator tracking into amplitude and phase errors thus providing a promising tool for quantitative assessment of real-time hybrid simulation results. Previous applications of FEI successfully evaluated actuator tracking over the entire duration of the tests. In this study, FEI with moving window technique is explored to provide post-experiment localized actuator tracking assessment. Both moving window with and without overlap are investigated through computational simulations. The challenge is discussed for Fourier Transform to satisfy both time domain and frequency resolution for selected length of moving window. The required data window length for accuracy is shown to depend on the natural frequency and structural nonlinearity as well as the ground motion input for both moving windows with and without overlap. Moving window without overlap shows better computational efficiency and has potential for future online evaluation. Moving window with overlap however requires much more computational efforts and is more suitable for post-experiment evaluation. Existing RTHS data from Network Earthquake Engineering Simulation (NEES) is utilized to further demonstrate the effectiveness of the proposed approaches. It is demonstrated that with proper window size, FEI with moving window techniques enable accurate localized evaluation of actuator tracking for real-time hybrid simulation.

Keywords: real-time hybrid simulation; frequency-domain evaluation index; tracking error; moving window

1. Introduction

Real-time hybrid simulation (RTHS) splits the prototype structure under investigation into experimental and analytical substructure(s), which allows researchers to observe the behavior of critical elements at large or full scale when subjected to dynamic loading (Nakashima *et al.* 1992, Blakeborough *et al.* 2001). A typical process of RTHS is schematically shown in Fig. 1, where the calculated displacements (x^c_i) from an integration algorithm are applied to both numerical and experimental substructures. Measured/calculated restoring forces (r^a_{i+1} and r^e_{i+1}) from the substructures are fed back to the numerical algorithm to compute structural response for next time step. Since this process is conducted in a real-time manner, RTHS provides an efficient and economical technique to account for rate-dependence within civil engineering structures in size-limited laboratories (Christenson *et al.* 2008, Chen *et al.* 2012, Chen *et al.* 2014, Asai *et al.* 2015, Friedman *et al.* 2015). After years of development, the RTHS technique has become a viable alternative for the more well-established shaking table testing method and the pseudo-dynamic testing method (Mahin *et al.* 1989, Kwon *et al.* 2008).

In RTHS, there are inevitable time delays due to communication, computation as well as actuator dynamics, resulting in unsynchronized displacements of experimental substructures with the calculated ones. Due to actuator delay, the forces of experimental substructures are measured before the actuators actually reach their target positions. Researches showed that actuator delay would lead to inaccurate test results and even destabilize the entire simulation if not compensated properly (Chen and Ricles 2009, Karavasilis *et al.* 2011, Gao *et al.* 2013). Various compensation methods have been proposed to avoid the instability caused by actuator delay and to improve actuator tracking. For conventional delay compensation methods of which the time delay is often assumed constant during test, their performances therefore depend on the accuracy of estimated delay, such as the polynomial extrapolation method and linear acceleration extrapolation (Horiuchi *et*
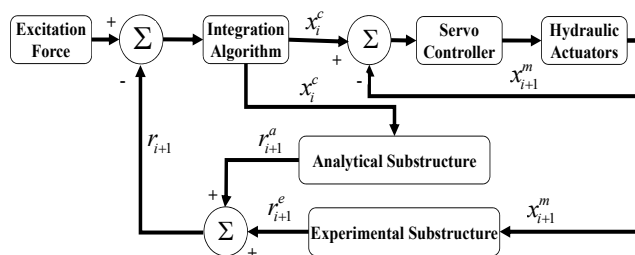

Fig. 1 Schematic representation of a real-time hybrid simulation

---

∗Corresponding author, Professor
 E-mail: chcsfsu@sfsu.edu
[a]Ph.D. Student
[b]Professor

al. 1999, Horiuchi and Konno 2001), the inverse compensation (Chen and Ricles 2008), and the model-based compensation (Carrion and Spencer 2006). Many efforts have been devoted to improve the performance of the delay compensation methods. The Darby estimator, for example, updates the estimated delay by calculating the error between the measured and the desired actuator positions (Darby *et al.* 2002). Chen and Ricles (2010) proposed adaptive inverse compensation (AIC) method, which adapts the parameters of the inverse compensation based on the trend of tracking indictor in the test. Phillips and Spencer (2012) modified the parameters of mode-based strategies to achieve desirable compensation by feed forward-feedback tracking control. Gao *et al.* (2013, 2014) developed a robust mode control for actuator based on H_∞ loop shaping design, which utilized both in single-degree-of-freedom (SDOF) and multiply-degree-of-freedom (MDOF) tests. Instead of associating the execution error with a variable or a constant delay, Elkhoraibi and Mosalam (2012) corrected the command signal according to actuator velocity.

Experimental studies however showed that the actuator delay can be reduced but cannot be completely eliminated even with sophisticated compensation methods. Thus, assessment of actuator tracking in RTHS becomes critical to ensure reliable experimental results for appropriate interpretation of structural performance under selected ground motions. Existing evaluation methods are mainly based on time domain analysis through comparing the command and measured displacements of the actuators, such as the maximum tracking error (MTE), root-mean-square (RMS) of the tracking error, tracking indicator (TI) (Mercan and Ricles 2007) and energy error (EE) (Mosqueda *et al.* 2007a, b). These variables can provide qualitative but not quantitative assessment on actuator tracking. Guo *et al.* (2014) proposed a frequency evaluation index (FEI) method to evaluate actuator tracking in terms of amplitude error and phase error. Using the concept of equivalent frequency, an equivalent time delay can be calculated quantitatively for the entire test. More recently, Guo *et al.* (2014) also proposed two decimation techniques to improve the computational efficiency of FEI. These findings show that the FEI method provides an efficient and effective way for post-experiment assessment of actuator tracking error.

For a typical seismic test, peak structural response often occurs within a short time window of 2 to 8 seconds, while the duration of the entire test could be as long as 120 seconds. Accurate actuator tracking during this short time window is critical for replicating structural response under earthquakes. This requires a tool for localized assessment of actuator tracking. In this paper, an FEI based technique is developed through Short Time Fourier Transform (STFT) for localized actuator tracking assessment. The localized evaluation is not intended to calculate the time delay at every millisecond, but to calculate the average delay within the short time window. When this window becomes small enough, the average delay in each window provides a truthful evaluation of the actuator tracking for RTHS. Moving windows with and without overlap are explored in this study to provide localized quantitative assessment of actuator tracking. Both computational simulations and existing laboratory tests are used to demonstrate the effectiveness of proposed method.

2. Frequency-domain evaluation indices

The FEI provides an effective way for quantitative post-experiment evaluation of actuator tracking errors. Utilizing the Fast Fourier Transform (FFT) in Eq. (1), the FEI interprets actuator tracking error in terms of amplitude and phase errors defined in Eq. (2) and Eq. (3), respectively

$$FEI = \sum_{j=1}^{p} \left\{ \frac{y_o(f_i)}{y_I(f_i)} \cdot \frac{\|y_I(f_i)\|^2}{\sum_{i=1}^{p} \|y_I(f_i)\|^2} \right\} \tag{1}$$

$$A = \|FEI\| \tag{2}$$

$$\phi = arc\tan\left[\text{Im}(FEI)/\text{Re}(FEI)\right] \tag{3}$$

Introducing the concept of equivalent frequency in Eq. (4), the equivalent delay can be calculated based on the phase error as Eq. (5)

$$f^{eq} = \frac{\sum_{i=0}^{p} (\|(y_I(f_i))\|^2 \cdot f_i)}{\sum_{i=0}^{p} \|(y_I(f_i))\|^2} \tag{4}$$

$$d = -\phi / (2\pi \cdot f^{eq}) \tag{5}$$

where $y_I(f)$ and $y_o(f)$ represent the FFT of the input $y_I(t)$ and output $y_o(t)$, respectively; A, ϕ, f^{eq} and d are generalized amplitude, phase, equivalent frequency and equivalent delay, respectively; p is the number of frequencies considered in the computation; and f_i is the ith frequency. For FFT, 2^p equals to the smallest power of two greater than or equal to the number of data points. To eliminate the effect of the spectrum leakage, the mean of both input and output signals should be removed and a Hanning window is applied before FFT. The closer A is to 1 and d is to 0, the more accurately the output signal replicates the input signal, implying better actuator tracking. The error between A and 1 is often referred to as amplitude error, while d is referred to as time delay. Under the circumstance of perfect actuator tracking, neither time delay nor amplitude error exists between input and output, i.e., $A=1$ and $d=0$.

3. FEI with moving window

3.1 Moving window technique

For signals with limited length, the Short Time Fourier Transform (STFT) (Bracewell 2000) can be expressed as

$$X(t,f) = \int_{-\infty}^{+\infty} \omega(t-\tau)x(\tau)e^{-j2\pi f\tau}d\tau \qquad (6)$$

where $\omega(t)$ is window function to reduce the effect of spectrum leakage; $x(\tau)$ and $X(t,f)$ are the signals in the time and frequency domain, respectively. In this study, a Hanning window is used in the FEI, which can be written as
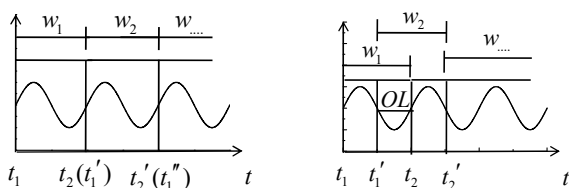
$$\omega(t) = \begin{cases} \dfrac{1}{2(t_2-t_1)}(1+\cos\dfrac{\pi(t-t_1)}{t_2-t_1}) & t_1 \le t \le t_2 \\ 0 & t < t_1, t_2 < t \end{cases} \qquad (7)$$

where t_1 and t_2 are the start time and the end time of the signal to be analyzed. According to Eq. (3), the window size t_w equals (t_2-t_1). The corresponding data length N equals the window size multiplying the sampling frequency. It is obvious that both the data length N and window size t_w refer to the same concept, where the former represents the number of data points and the latter is the length of window in time.

The moving windows are applied in two different ways, namely moving window without overlap (MW) and moving window with overlap (MWO). As shown in Fig. 2, the end time t_2 of existing window is the start time t_1 of the next window for windows without overlap, while for windows with overlap the end time t_2 is larger than the start time t_1 of the next window.

One of the disadvantages of the STFT is that the data length of the window determines the frequency resolution (the smallest frequency that can be identified from STFT) and time resolution (the time duration to identify variation within the signal). The width of the windowing function relates to how the signal is represented-it determines whether there is good frequency resolution (i.e., frequency components close together can be separated) or good time resolution (i.e., the time at which frequencies change). A wide window gives better frequency resolution but poor time resolution. A narrow window however gives good time resolution but poor frequency resolution.

The conversion from continuous time to samples (discrete-time) changes the underlying Fourier transform of $x(t)$ into a discrete-time Fourier transform (DTFT), which generally entails a type of distortion called aliasing. Choice of an appropriate sampling rate is the key to minimizing the effect of aliasing. Similarly, the conversion from a very long (or infinite) sequence to a manageable size entails a type of distortion called leakage, which is manifested as a loss of resolution in the DTFT. Choice of an appropriate window

length is the primary key to minimize the effect of spectrum leakage. The DTFT is not reliable if the available data (and time to process it) is less than the amount needed to attain the desired frequency resolution (Bracewell 2000). Better time resolution, on the other hand, requires smaller data window, satisfying the frequency resolution. To be more specific, the window should be long enough to guarantee the frequency resolution, while the window length should also be short enough to ensure sufficient time resolution.

3.2 Window size for MW

The window length for the FFT should be an integer power of two and, if not, will have zeros patched to the end of the signals. Thus, the window size t_w and frequency interval Δf for the FEI become

$$t_w = N / f_s \qquad (8a)$$

$$\Delta f = f_s / 2^{nextpow2(N)} \qquad (8b)$$

where $2^{nextpow2(N)}$ is the smallest power of two that is greater than or equal to the data length N. According to Eqs. (8a) and (8b), a larger window size of t_w leads to better frequency resolution.

To find appropriate window size that provides acceptable time and frequency resolution, computational simulations of a SDOF structure are conducted using delay differential equation model (Wallace *et al.*). The mass of the structure is 1000 kg, and the inherent viscous damping ratio of the SDOF structure is assumed to be 2%. The natural frequency of the structure varies from 0.2 Hz to 5.1 Hz with an increment of 0.1 Hz. The amplitude k_p and time delay τ have constant values of 1 and 1 msec., respectively. Ten different ground motions are randomly selected from the Pacific Earthquake Engineering Research (PEER) Strong Motion Database, and the sampling rate is 1024 Hz. The window size t_w increases from the natural period of the structure with an increment of ten percent of natural period until the error between calculated time delay using the FEI and the theoretical value is less than 5% (i.e., 0.05 msec.). The variation of the desired window size t_w with respect to the structural natural frequency and period are presented in Fig. 3.

As can be observed from Fig. 3(a), the window size to achieve accurate analysis varies with respect to the natural frequency of the structure. For the same ground motion, the lower the natural frequency is, the larger the window size should be. For the same natural frequency/period, the window size varies for different ground motions to achieve good accuracy. It can also be observed in Fig. 3(b) that accurate results can be achieved when the window size is between two and four times of the natural period for linear elastic structures.

3.3 Overlap for MWO

To guarantee the accuracy of the FEI with MW, the window size t_w should be at least twice the fundamental period of the structure. For structures with low natural

(a) MW	(b) MWO

Fig. 2 Two moving window techniques

(a) Wind speed profile   (b) Wind direction profile
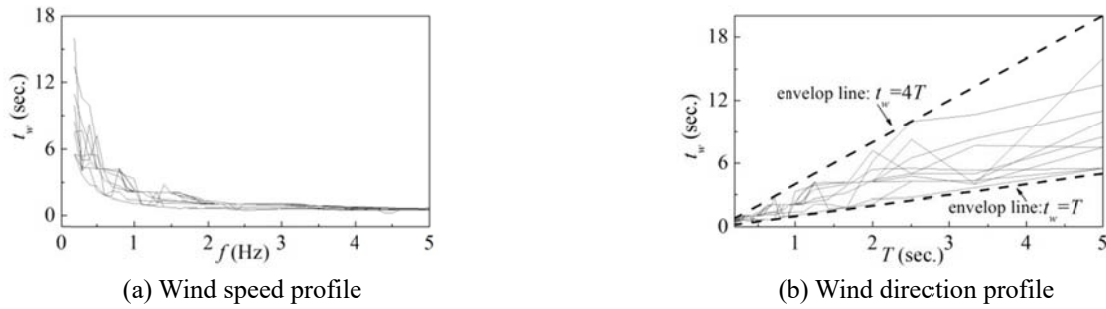
Fig. 3 The variation of the desired window size t_w with respect to structural natural frequency and period

frequencies, good frequency resolution can be achieved but with poor time resolution. To overcome this, a moving window with overlap shown in Fig. 2(b) is explored using FEI for more detailed localized assessment of actuator tracking. Assuming that the overlap length between two adjacent windows is *OL*, the MWO is the same as MW when *OL* equals 0. The larger the *OL* is, the more details the FEI will derive. Thus, *OL* should be selected to be the largest possible value as following,

$$OL = N - 1 \qquad (9)$$

Using the overlap length in Eq. (9), the amplitude error and time delay of FEI can be calculated for every sampling time. It however should be noted that, the larger *OL* is, the more computational effort is required. It should also be noted that OL can be any value between zero and the data length of the window.

4. Computational simulation

To verify the effectiveness of the FEI based moving window techniques, computational simulations are conducted to emulate RTHS of both linear and nonlinear structures. The Bouc-Wen model (1980) is used to emulate the restoring force for nonlinear structure as following

$$r^a(t) = \eta \cdot k_a \cdot x^a(t) + (1-\eta) \cdot k_a \cdot x_y^a \cdot z(t) \qquad (10a)$$

$$x_y^a \cdot \dot{z}(t) + \gamma \left| \dot{x}^a(t) \right| \cdot z(t) \cdot \left| z(t) \right|^{q-1} + \beta \cdot \dot{x}^a(t) \cdot \left| z(t) \right|^q$$
$$- \dot{x}^a(t) = 0 \qquad (10b)$$

where $x_{a,y}$ is the yield displacement and set to 10 mm; k_a is the linear elastic stiffness of the analytical substructure and is set to 11.765 kN/mm; η is the ratio of the post- to pre-yield stiffness of the analytical substructure and is set to 0; $x^a(t)$ is the displacement imposed on the analytical substructure by the integration algorithm; and $z(t)$ is the evolutionary parameter of the Bouc-Wen model and the dimensionless parameters β, γ, q control the shape of the hysteretic loop of the analytical substructure, the values of the parameters are set to 0.55, 0.45 and 2, respectively.

For the purpose of demonstration, three fundamental frequencies of the SDOF structure are selected including 0.5 Hz, 0.7 Hz and 1.0 Hz, which correspond to the natural period of 2 sec., 1.4 sec. and 1 sec., respectively. It should

also be noted that similar results could also be derived for other frequencies. The time delay and amplitude error between calculated displacement and measured displacement are 5 msec. and 1.1, respectively. The CAP000 component recorded at Capitola station during the 1989 Loma Prieta earthquake is selected from the PEER Strong Motion Database (2008) with the peak ground acceleration of 0.0528 g. The measured displacements for both linear and nonlinear structure are presented in Figs. 4(a) and 4(b), where nonlinear structural behavior can be observed in Fig. 4(b) when the displacement response exceeds the yield displacement of 10 mm. The maximum displacement responses are 26 mm, 39 mm and 84 mm for 0.5 Hz, 0.7 Hz and 1 Hz structures, respectively, which correspond to 2.6, 3.9 and 8.4 times of the yield displacement, respectively.

4.1 MW technique

Since the window size should be at least twice the natural period of the structure, the window sizes t_w are selected as 2.0 sec. (N=2048), 2.8 sec. (N=2867) and 4.0 sec. (N=4096). The corresponding frequency intervals for DFTF are 0.5 Hz, 0.25 Hz and 0.25 Hz, respectively. Figs. 5(a) and 5(b) show the analysis results for the SDOF structure with natural frequency of 0.5 Hz. The amplitudes in Fig. 5(a) are observed to vary from 1.08 to 1.11 and the time delay in Fig. 5(b) varies from 3.5 msec. to 5.0 msec. when the window sizes t_w is 2.0 sec. (N=2048). Better performance can be observed for the window sizes t_w of 2.8 sec. (N=2867), where the amplitudes vary from 1.09 to 1.11 and the time delays vary from 4.2 msec. to 5.2 msec.. The amplitude and time delay of the linear structure are almost identical with theoretical values for the window size of 4.0 sec. (N=4096). With the window size twice the natural period, the FEI with MW is observed to provide accurate localized assessment of actuator tracking for RTHS of linear elastic structures. Similar observations can be made for the FEI with MW applied to nonlinear structure in Figs. 5(c) and 5(d). The window size of 4.0 sec. provides the best accuracy of tracking assessment. The maximum errors between the calculated indices and the theoretical ones are presented in Table 1. It can be observed in Table 1 that for the linear structure, when the window size increases from 2.0 seconds to 4.0 seconds, the maximum errors decrease significantly from 1.1% to 0.3% for amplitude *A* and from 27.0% to 6.4% for time delay *d*. For the nonlinear structure,
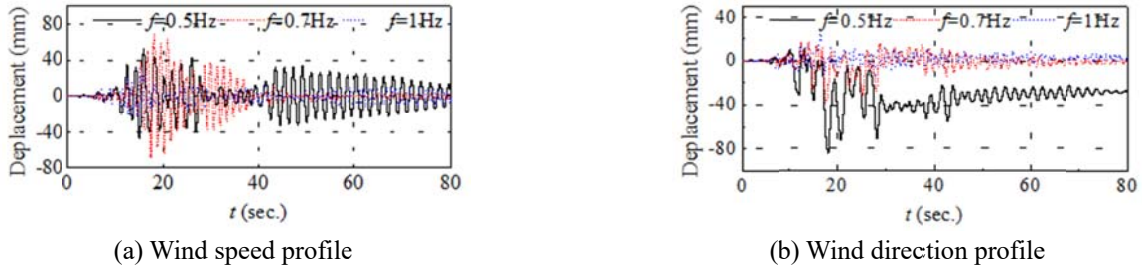
(a) Wind speed profile

(b) Wind direction profile

Fig. 4 The variation of the desired window size t_w with respect to structural natural frequency and period

(a) A for linear structure

(b) d for linear structure

(c) A for nonlinear structure
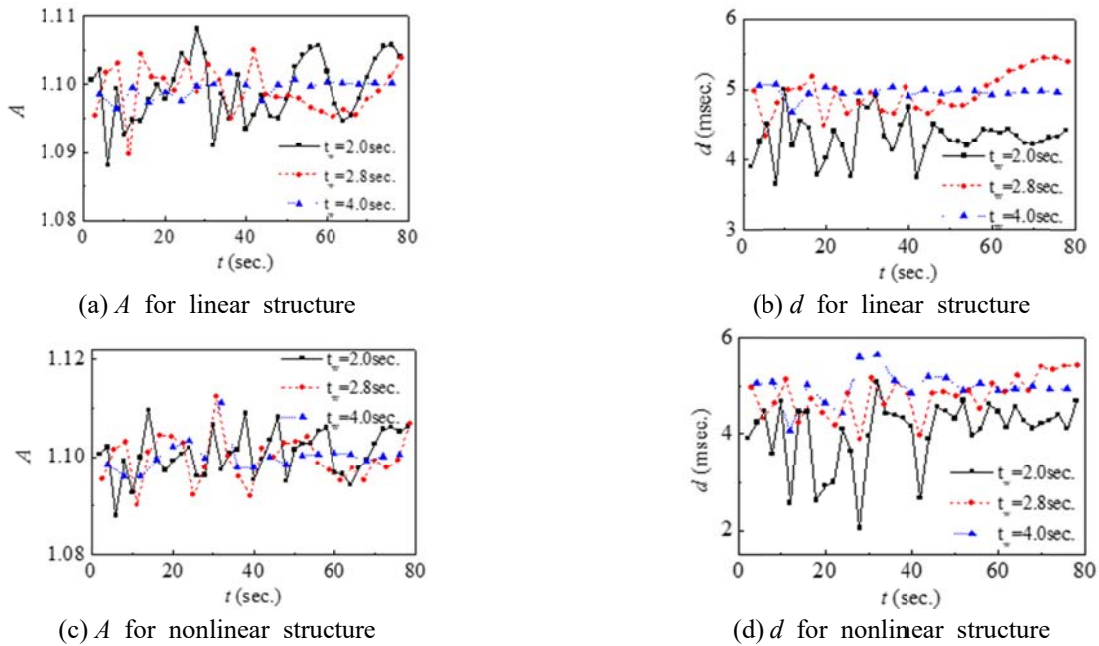

(d) d for nonlinear structure

Fig. 5 Analysis results for SDOF structure with natural frequency of 0.5 Hz

Table 1 Maximum error (%) of calculated FEI indices for SDOF structure with natural frequency of 0.5 Hz

Window size	Linear structure		Nonlinear structure	
	A	d	A	D
2.0 sec.	1.1	27.0	1.1	59.0
2.8 sec.	0.9	13.2	1.1	22.2
4.0 sec.	0.3	6.4	1.0	18.3

Table 2 Maximum error (%) of calculated FEI indices for SDOF structure with natural frequency 0.7 Hz

Window size	Linear structure		Nonlinear structure	
	A	d	A	d
2.0 sec.	0.9	6.4	0.6	8.2
2.8 sec.	0.5	4.0	0.4	4.1
4.0 sec.	0.4	1.0	0.3	2.4

the maximum error for d reduces quickly from 59.0% to 18.3% when the window size increases from 2.0 seconds to 4.0 seconds. The maximum amplitude error remains almost the same around 1.0%. The maximum errors are observed to be larger for nonlinear structure when compared with those for linear structure, which indicates that nonlinear structures require larger window length for accurate analysis results.

For the structure with natural frequency of 0.7 Hz, the analysis results with different window sizes are presented in Fig. 6. Compared with those in Fig. 5 for the structure with natural frequency of 0.5 Hz, the analysis results are more accurate for the structure with natural frequency of 0.7 Hz. Similarly, it can be observed from Fig. 6 that the larger the window size, the better accuracy of the analysis results for both linear structure and nonlinear structure. The maximum

errors are presented in Table 2 for the calculated indices.

From Table 2, the maximum errors of the calculated indices decrease when the window size increase from 2.0 sec. to 4.0 sec. for both linear structure and nonlinear structure. Compared with those for 0.5 Hz structure in Table 1, the analysis results for 0.7 Hz structure are much better.

The maximum amplitude and delay error are less than 0.5% and 5% for both linear structure and nonlinear structure when the window size is twice the fundamental period of the structure. Again the maximum errors of indices d are observed to be larger for nonlinear structure when compared with those for linear structure.

For the structure with natural frequency of 1.0 Hz, the analysis results are presented in Fig. 7. Compared with those presented in Figs. 5 and 6, Fig. 7 shows the best performance for the same window length. The calculated
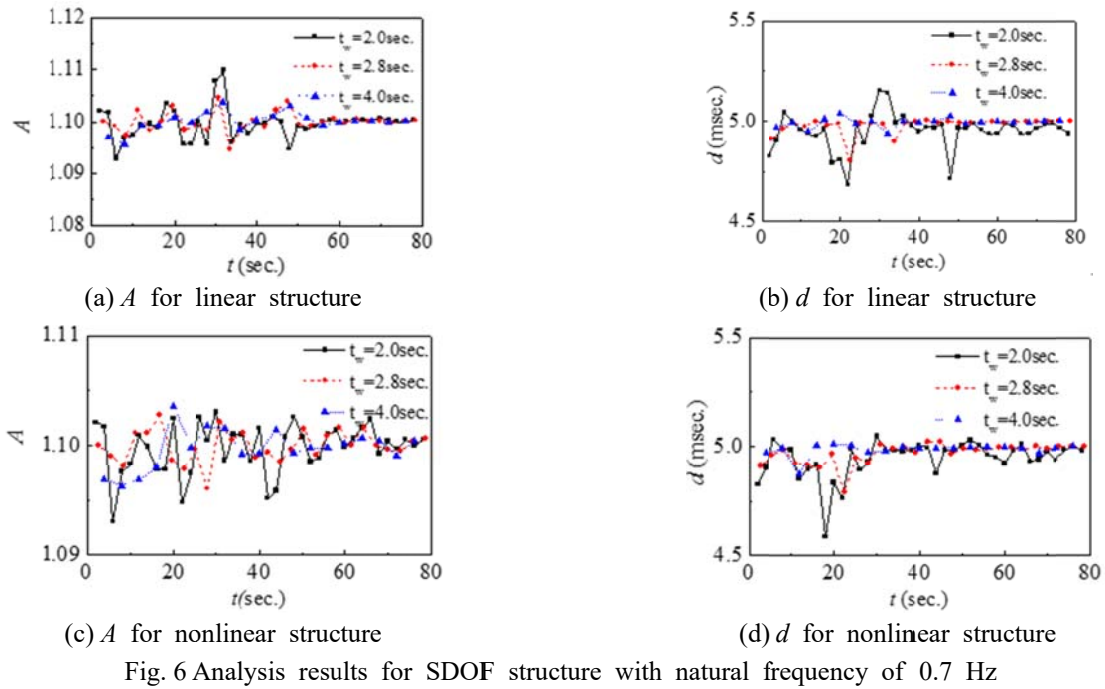
(a) *A* for linear structure

(b) *d* for linear structure

(c) *A* for nonlinear structure

(d) *d* for nonlinear structure

Fig. 6 Analysis results for SDOF structure with natural frequency of 0.7 Hz

(a) *A* for linear structure

(b) *d* for linear structure

(c) *A* for nonlinear structure
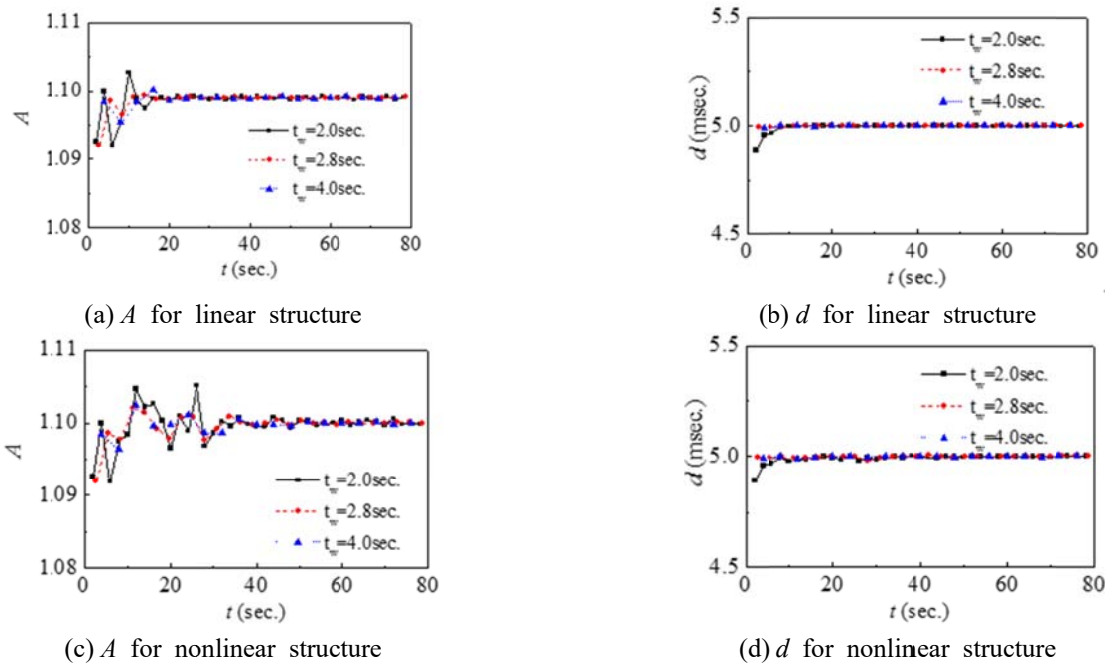

(d) *d* for nonlinear structure

Fig. 7 Analysis results for SDOF structure with natural frequency of 1.0 Hz

Table 3 Maximum error (%) of calculated FEI indices for SDOF structure with natural frequency 1.0 Hz

Window size	Linear structure		Nonlinear structure	
	A	*d*	*A*	*d*
2.0 sec.	0.7	2.3	0.7	2.2
2.8 sec.	0.7	0.1	0.7	0.4
4.0 sec.	0.4	0.3	0.3	0.3

amplitude and time delay for both linear structure and nonlinear structure are almost identical with theoretical values. The maximum errors between the calculated and the theoretical indices are presented in Table 3

It can be observed from Table 3 that the maximum errors in amplitude and delay errors are less than 1% and 2.5%, for both linear structure and nonlinear structure, respectively, when the window size is larger than the two times of the fundamental period of the structure. For the linear structure, when the window size is twice the natural period, the maximum errors for amplitude are 0.3%, 0.5%, 0.7%, and the maximum delay error are 6.4%, 4.0% and 2.3% for the structures with natural frequency of 0.5 Hz, 0.7 Hz and 1 Hz, respectively. Thus, twice of the natural period is suitable for RTHS of linear structure under these cases.
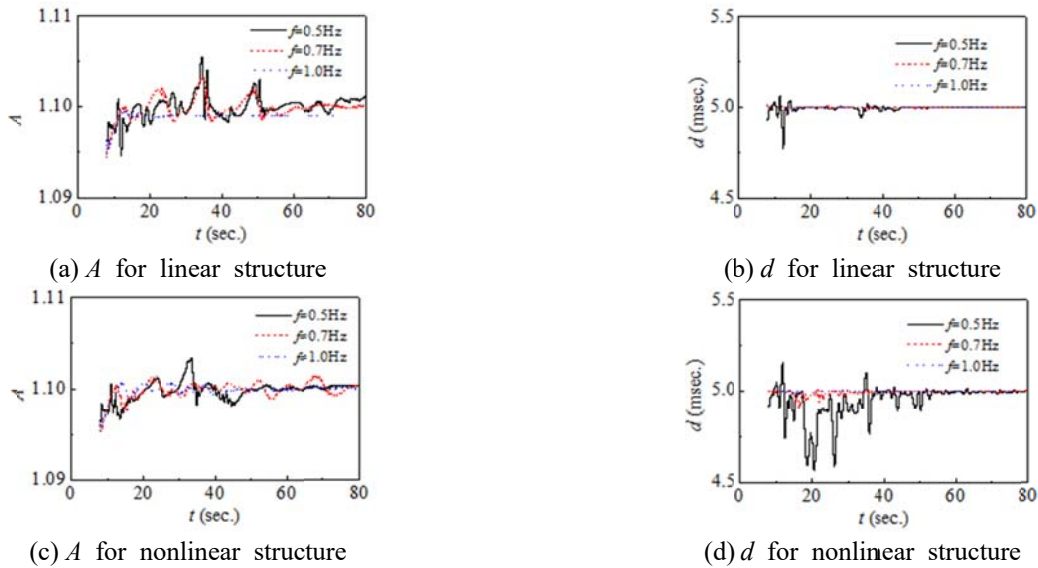
(a) A for linear structure

(b) d for linear structure

(c) A for nonlinear structure

(d) d for nonlinear structure

Fig. 8 Analysis results for SDOF structures using FEI with MWO

Table 4 Average computation time for FEI with MW

Window size (sec.)	2.0	2.8	4.0
Computational time (msec.)	37.9	36.5	28.4

However, a maximum delay error up to 18.3% is observed for nonlinear structure with natural frequency of 0.5 Hz when the window size is twice the natural period. This can be attributed to the fact that the structure develops significant nonlinearity in Fig. 4(b), where the maximum displacement is more than eight times of the yield displacement. Thus, for nonlinear structure, the same window size as for the linear structure can be used when the nonlinearity is not significant, such as when the maximum displacement is smaller than 4 times of the yield displacement. However, larger window size is necessary for localized evaluation for RTHS involving significant nonlinearity, such as when the maximum displacement is larger than 8 times of the yield displacement.

There are three types of window sizes in above analysis and six simulations are conducted for each window size. The computer used for simulations has the CPU of Intel i5-3470, and 8GB of RAM. The computation time is similar for all simulations with same window size and the average computation time is presented in Table 4. It can be observed that the computation time can be ignored when compared with duration of the entire simulation, which implies that FEI with MW has potential to be applied in future online evaluation.

4.2 MWO technique

To improve the accuracy of analysis for structures with low frequency and/or strong nonlinearity, FEI with MWO is explored in this section. As can be observed in Fig. 4, the displacements are relatively small in first 12 sec. for both linear structure and nonlinear structure under different frequencies. The performance of the simulation after 12 sec. is more important for structural performance evaluation.

Thus, the window size t_w is selected as 8.0 sec. (N=8192) with the overlap OL equals 8191. As a result, the analysis results are not available for the first 8.0 sec., while the test can be analyzed for every 1/1024 second after the 8.0 sec.

The analysis results using FEI with MWO for structures with different frequencies are presented in Fig. 8. As can be observed in Figs. 8(a) and 8(c), the errors between calculated and theoretical amplitudes are less than 1%, which shows the advantages of the moving window with overlap. Moreover, it is also observed that the analysis results for structure with higher natural frequency are more accurate. Similar observation can also be made in Fig. 8(b) and 8(d). The relatively large oscillation in Fig. 8(d) when the frequency is 0.5 Hz is mainly due to the nonlinearity of the structure. The maximum errors of the calculated indices using FEI with MWO are presented in Table 6.

It can be observed that the maximum errors of the calculated indices decrease with the frequency of the structure when the window size is same for both linear structure and nonlinear structure. Compared with those in Tables 1 to 3 using FEI with MW, the analysis using FEI with MWO provide more accurate results, especially when the structure develops nonlinear behavior. A maximum error of 8.8% is observed in time delay d for FEI with MW when applied to the nonlinear structure with natural frequency of 0.5 Hz. From Fig. 8(d), the maximum delay error occurs around 20 sec., which corresponds to the maximum displacement in Fig. 4(b). Thus, it can be concluded that FEI with MWO provides better accuracy for strongly nonlinear structure. Since the above three simulations are analyzed by same window size and overlap length when using MWO, the computation time for these simulations are almost the same, which can be as large as 177 sec.. This computation time, compared with that of FEI with MW, could make it difficult if not impossible to implement for on-line actuator tracking evaluation. FEI with MWO therefore could be more appropriate for post-experiment evaluation.
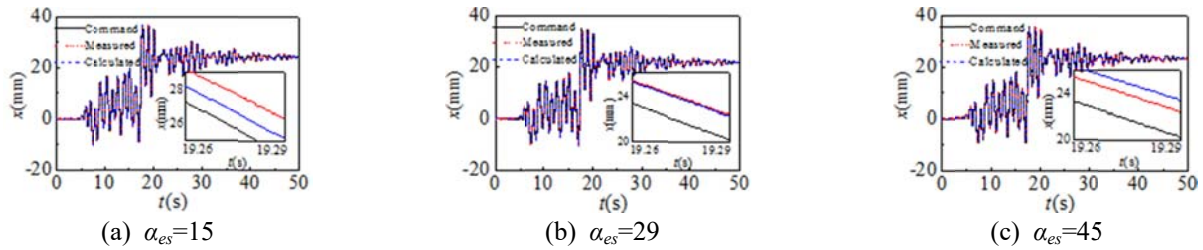
(a) α_{es}=15   (b) α_{es}=29   (c) α_{es}=45

Fig. 9 Displacement responses for project 711

(a) A (α_{es}=15)   (b) d (α_{es}=15)   (c) A (α_{es}=29)

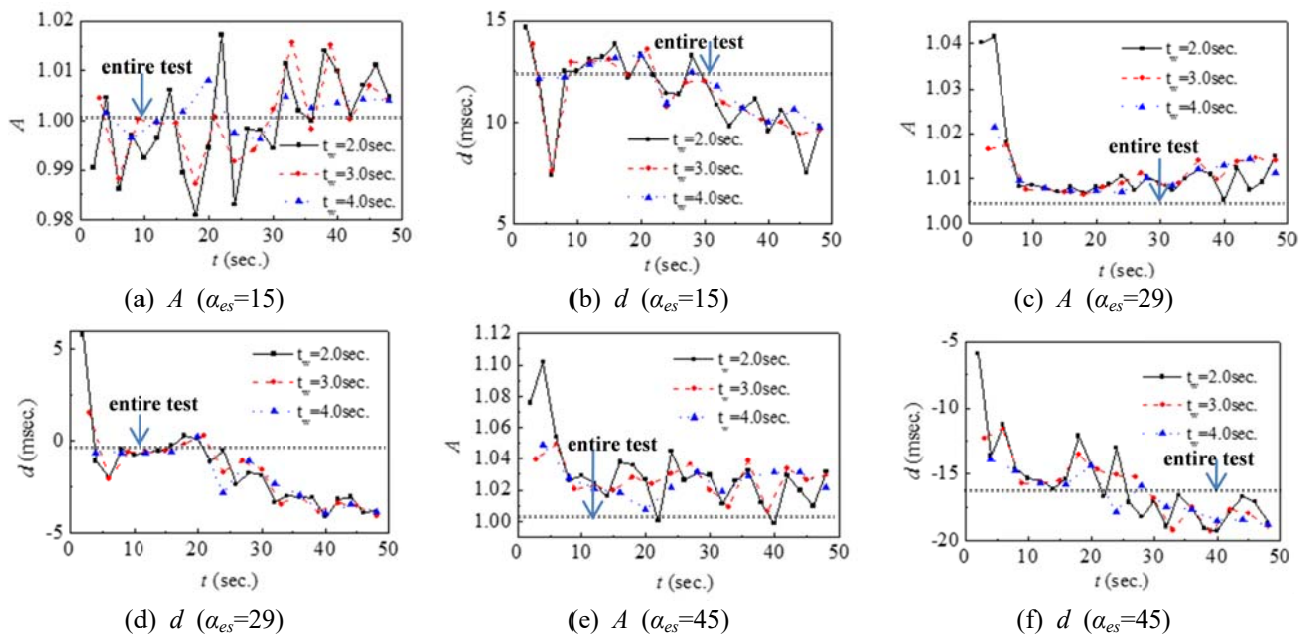(d) d (α_{es}=29)   (e) A (α_{es}=45)   (f) d (α_{es}=45)

Fig. 10 Localized evaluation using FEI with MW for the project 711

Table 6 Maximum error (%) of calculated indices for FEI with MWO

Frequency	Linear structure		Nonlinear structure	
	A	d	A	d
0.5 Hz	0.5	1.4	0.3	8.8
0.7 Hz	0.5	0.3	0.4	1.8
1.0 Hz	0.6	0.1	0.4	0.2

5. Experimental verification

5.1 Data source and experiments description

Experimental data from two projects in NEEShub (Ricles 2008, Friedman *et al.* 2013) are analyzed to further demonstrate the effectiveness of the moving window technique for localized evaluation. The Project 711 (Ricles 2008) aimed at establishing real-time testing capabilities with advanced servo-hydraulic control at the Lehigh University NEES Equipment Site for testing of structural systems with dampers. Three experiments are selected including the first, fourth and seventh experiments, where estimated time delay α_{es} are 15 msec., 29 msec. and 45 msec., respectively. The Project 648 (Friedman *et al.* 2013) intended to validate the performance of a new semi-active control algorithm, identify the braced frame and design two

actuator delay compensation schemes. The test data labeled as COC_100_LA44_I0p5 in the third hybrid simulation is considered in this study.

5.2 Analysis results for project 711

For project 711, the analytical substructure is the SDOF MRF, which has a mass of 503.4 metric tons, an elastic natural frequency of 0.77 Hz, and an inherent viscous damping ratio of 0.02. The experimental substructure is an elastomeric damper. The restoring force of the SDOF MRF is emulated using the same Bouc-Wen model in Eqs. 10(a) and 10(b). The N169E component of the 1994 Northridge earthquake recorded at Canoga Park was selected as the ground motion, and the maximum ground acceleration was scaled to 0.322m/s² to satisfy the limits imposed by the servo-hydraulic equipment. The unconditionally stable explicit CR integration algorithm was used for the real-time hybrid simulations. The inverse compensation method with different actuator delay estimates (15 msec., 29 msec. and 45 msec.) was used to negate the effect of servo-hydraulic dynamics.

Closed-up views of the displacement responses are presented in Fig. 9. The amplitude A and time delay d from frequency-domain evaluation are presented in Table 7 when applying the FEI for the entire duration of tests. The

Table 7 FEI analysis of entire test duration for Project 711

α_{es}	A	d (msec.)
15	1.003	12.3
29	1.001	-1.1
45	1.005	-16.2

(a) A (b) d

Fig. 11 Localized evaluation using FEI with MWO for the project 711

amplitude errors for all three tests are observed to be less than 0.5%. The equivalent time delay is identified as 12.3 msec. for the test with α_{es} is equal to 15, indicating that the measured displacement generally lags behind the calculated displacement about 12.3 msec.. When α_{es} equals 29, the equivalent delay is -1.1 msec., implying that the measured displacement generally leads the calculated displacement about 1.1 msec.. When α_{es} equals 45, the equivalent delay is -16.2 msec., indicating that the measured displacement generally leads the calculated displacement about 16.2 msec.. Based on the FEI analysis of entire duration of the three tests, it can be derived that the test with α_{es} is equal to 29 provides the best actuator tracking of all three tests, thus providing the most reliable results in replicating the structural response under selected ground motion.

5.2.1 Analysis of experimental results using the MW technique

As the natural frequency of the prototype structure is 0.77 Hz, three different window sizes are selected including 2 sec., 3 sec. and 4 sec., which give FEI indices of A and d every two, three and four seconds, respectively. The analysis results are presented in Fig. 10. For the purpose of comparison, also presented in Fig. 10 are the values of amplitude and equivalent time delays derived from frequency-domain evaluation of the entire duration of tests.

As can be observed from Fig. 10, the amplitude A and time delay d vary throughout the entire duration of all three tests. The amplitudes are larger than 1 for tests with α_{es} equal 29 and 45 in Fig. 10(c) and Fig. 10(e), while the test with α_{es} equals 15 is observed to have some of the amplitude values smaller than 1.0 in Fig. 10(a). Both tests with α_{es} equal 29 and 45 are observed to have large values of amplitude at the beginning of the tests. The values of time delay d are observed in Fig. 10(b) to be larger than 5 msec. throughout the test when α_{es} equals 15, while smaller than -5 msec. in Fig. 10(f) when α_{es} equals 45. This is consistent with the findings in Table 7 that the test with α_{es} equals 15 is under-compensated while the test with α_{es} equals 45 is over-compensated. The values of d are observed in Fig. 10(d) to vary between -5 msec. and 5 msec. for the test of α_{es} equals 29.

Compared with FEI results of entire duration of tests in Table 7, the localized evaluation using moving window without overlap can have difference in amplitude up to 10% in Fig. 10(e), and difference in time delay more than 400% in Fig. 10(d). This indicates the importance of localized evaluation for real-time hybrid simulation. A further look into the displacement response indicates that the structure developed nonlinear behavior after 10 sec. with peak displacement around 20 sec.. Thus, displacement response between 10 and 20 sec. is more critical for structural
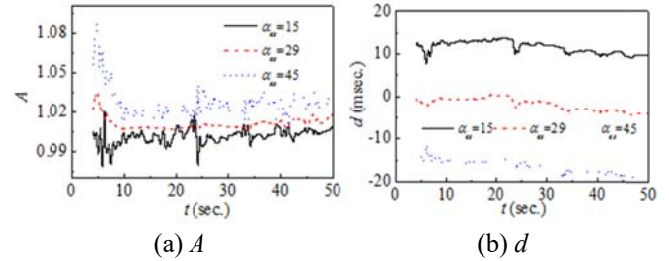
performance evaluation. From Figs. 10(a), (c) and (e), the amplitude A is closest to one between 10 and 20 sec. for the test with α_{es} equals 29. Similarly, the values of time delay d are closest to zero for the test with α_{es} equals 29, as can be observed in Figs. 10(b), (d) and (f). This indicates that the test with α_{es} of 29 provides most reliable results among all three tests.

5.2.2 Analysis of experimental results using the MWO technique

In this section, moving window with overlap is considered to further evaluate the tests from Project 711. The window size is 4.0 sec. (N=4096) with the overlap OL equals 4095, which gives analysis results of A and d every 1/1024 second. The amplitude and time delay of the tests are presented in Fig. 11. The amplitudes in Fig. 11(a) vary around 1.0 for all three tests and are observed to increase with respect to the value of α_{es}. Similar to those in Figs. 10(b), 10(d) and 10(f), the time delays in Fig. 11(b) are observed to be around 10 msec., -1.0 msec. and -15 msec. for the tests with α_{es} equal 15, 29, and 45, respectively. It can also be concluded that the test with α_{es} of 29 provides most reliable results among all three tests.

5.2 Analysis results for project 648

Table 8 presents the amplitude A and equivalent delay d from FEI analysis of test results over entire duration for project 648. The amplitude errors for all three tests are less than 1.5%. The equivalent time delays are 4.1 msec. and 6.5 msec. for Act1 and Act3, respectively, which indicates under-compensation for these two actuators. The time delay for Act2 is 0.7 msec., which is the smallest among the three actuators. Closed-up views are shown in Fig. 12 for the calculated, command, and measured displacements in first 30 seconds as well as in the last 25 seconds. It can be observed that the measured displacements are synchronous with calculated displacements in the first 30 seconds but asynchronous in the last 25 seconds for all three actuators.

Table 8 FEI analysis of entire test duration for Project 648

Actuator	A	d (msec.)
Act1	0.9878	4.1
Act2	0.9912	0.7
Act3	1.0019	6.5

(a) Act1   (b) Act2   (c) Act3

Fig. 12 Displacement responses for project 648

(a) *A* (Act1)   (b) *d* (Act1)   (c) *A* (Act2)

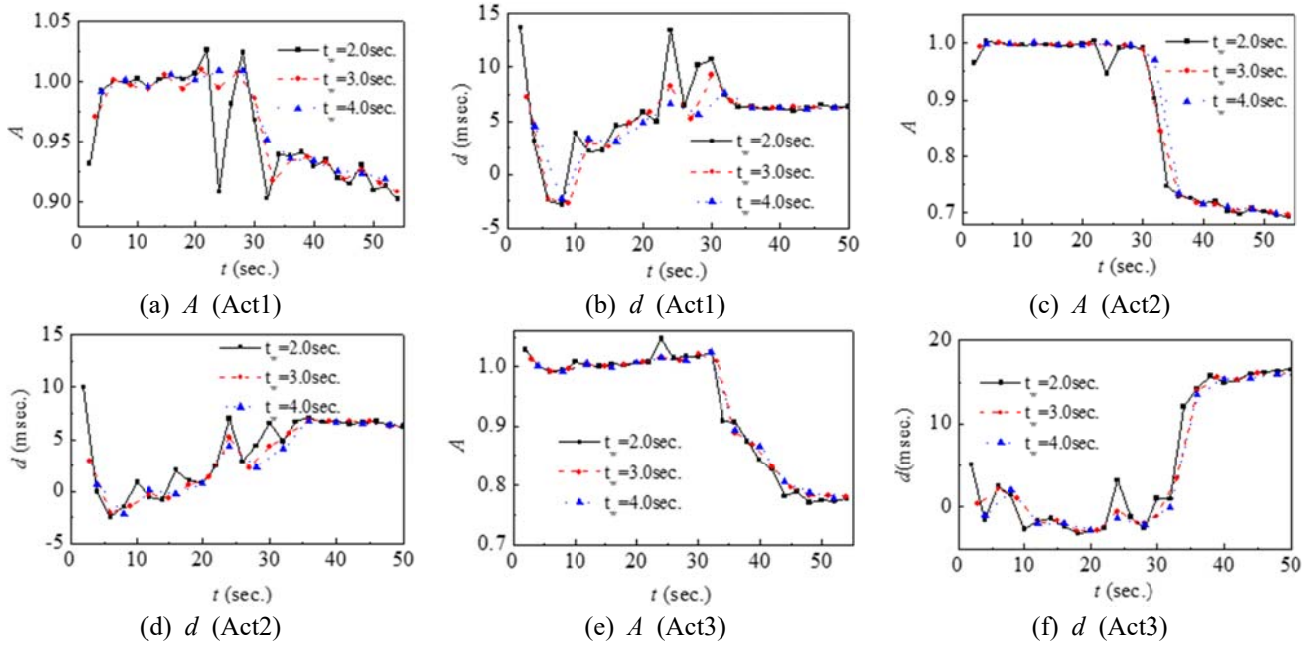(d) *d* (Act2)   (e) *A* (Act3)   (f) *d* (Act3)

Fig. 13 Localized evaluation using FEI with MW for the project 648

Thus, analysis results in Table 8 might not provide accurate assessment of actuator tracking and localized evaluation is necessary.

5.3.1 Analysis of experimental results using the MW technique

The window sizes are selected as 2 sec., 3 sec. and 4 sec. for each actuator. The analysis results are presented in Fig. 13. Both the amplitude *A* and time delay *d* are observed to vary throughout the test. Results from analysis with window size of 3.0 seconds are almost identical with those window size of 4.0 seconds. From Figs. 13(a), (c) and (e), the amplitudes for all three actuators are all around 1.0 before 30 sec., but decrease to 0.9 (Act1 in Fig. 13(a)), 0.7 (Act2 in Fig. 13(c)) and 0.8 (Act3 in Fig. 13(e)) after 30 sec.. Similarly, the time delays for all three actuators are around 0 before 30 sec., but increase to 6 sec. (Act1 in Fig. 13(a) and Act2 in Fig. 13(c)) and 18 sec. (Act3 in Fig. 13(e)) after 30 sec.. The amplitude and time delay for the three tests are consistent with the closed-up views of the displacement responses in Fig.12, which indicates the compensation method works much better in the first 30 seconds than in the last 25 seconds.

5.3.2 Analysis of experimental results using the MWO technique

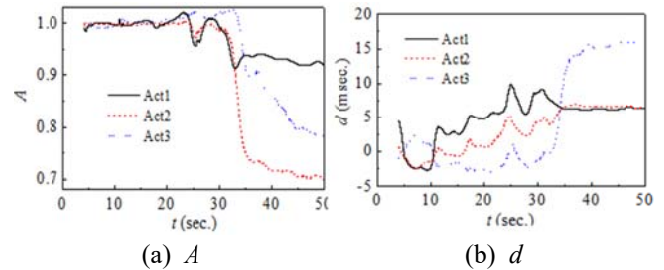(a) *A*   (b) *d*

Fig. 14 Localized evaluation for the project 648 using FEI with M

FEI with MWO is considered to further evaluate the performance of the actuators with the window size of 4.0 sec. (*N*=4096) and the overlap length of 4095. The analysis results are shown in Fig. 14. Similar to Fig. 13, good actuator tracking is observed in Fig. 14 for all three actuators in the first 30 seconds, and larges values of amplitude error and time delay are observed for the last 25 seconds.

6. Conclusions

Accurate actuator tracking evaluation is critical for reliability assessment of real-time hybrid simulation results

to appropriately interpret structural performance under earthquakes. The FEI has been demonstrated to provide good assessment of actuator tracking over the entire test duration. In RTHS, the peak structural response often occurs within a short time window, while the duration of the entire test could very long. Thus, a tool for localized assessment of actuator tracking is required. In this study, the FEI is further developed to integrate with moving window technique to provide accurate localized post-experiment assessment of actuator tracking. Computational simulations are conducted to determine the window length and verify the effectiveness of moving windows with or without overlap. Existing real-time hybrid simulation results are utilized to further demonstrate the effectiveness of the proposed approaches.

With appropriate window size, both moving window with and without overlap can provide good localized evaluation. Moving window without overlap does not need much computational effort, therefore has great potential for future online evaluation. Moving window with overlap has better time resolution but requires more computational efforts, which make it more suitable for post-experiment evaluation. The required window size depends on the natural frequency and structural nonlinearity as well as the ground motion input. The larger natural period and stronger nonlinearity of the structure, the larger window length is required in localized evaluation. The time length of the window should be more than twice the fundamental period for linear structure to balance the time resolution and accuracy of the analysis results

Acknowledgments

References

Asai, T., Chang, C.M. and Spencer, B.F. (2015), "Real-time hybrid simulation of a smart base-isolated building", *J. Eng. Mech.*, ASCE, **141**(3), 04014128.

Blakeborough, A., Williams, M.S., Darby, A.P. and Williams, D.M. (2001), "The development of real-time substructure testing", *Philos. T. Roy. Soc. A.*, **359**(1786), 1869-1891.

Bracewell, R.N. (2000). *The Fourier Transform and Its Applications*, (7th Edition), McGraw-Hill, Boston, MA, USA.

Carrion, J.E. and Spencer, B.F. (2006), "Real-time hybrid testing using model-based delay compensation", *Proceedings of the 4th International Conference on Earthquake Engineering*, Taipei, October.

Chen, C. and Ricles, J.M. (2008), "Stability analysis of SDOF real-time hybrid testing systems with explicit integration algorithms and actuator delay", *Earthq. Eng. Struct.*, **37**(4), 597-613.

Chen, C. and Ricles, J.M. (2009), "Analysis of actuator delay compensation methods for real-time testing", *Eng. Struct.*, **31**(11), 2643-2655.

Chen, C. and Ricles, J.M. (2010), "Tracking error-based servo-hydraulic actuator adaptive compensation for real-time hybrid simulation", *J. Struct. Eng.*, ASCE, **136**(4), 432-440.

Chen, C., Ricles, J.M., Karavasilis, T., Chae, Y. and Sause, R. (2012), "Real-time hybrid simulation system for performance evaluation of structures with rate dependent devices subjected to seismic loading", *Eng. Struct.*, **35**, 71-82.

Chen, P.C., Tsai, K.C. and Lin, P.Y. (2014), "Real-time hybrid testing of a smart base isolation system", *Earthq. Eng. Struct.*, **43**(1), 139-158.

Christenson, R., Lin, Y.Z., Emmons, A. and Bass, B. (2008), "Large-scale experimental verification of semi-active control through real-time hybrid simulation", *J. Struct. Eng.*, ASCE, **134**(4), 522-534.

Darby, A.P., Blakeborough, A. and Williams, M.S. (2002), "Stability and delay compensating for real-time substructure testing", *J. Eng. Mech.*, ASCE, **128**(12), 1276-1284.

Elkhoraibi, T. and Mosalam, K.M. (2012), "Towards error free hybrid simulation using mixed variables", *Earthq. Eng. Struct.*, **36**(11), 1497-1522.

Friedman, A., Dyke, S.J., Phillips, B., Ahn, R., Dong, B.P., Chae, Y., Castaneda, N., Jiang, Z.S., Zhang, J.Q., Cha, Y.J., Ozdagli, A.I., Spencer, B.F., Ricles, J.M., Christenson, R., Agrawal, A. and Sause, R. (2015), "Large-scale real-time hybrid simulation for evaluation of advanced damping system performance", *J. Struct. Eng.*, ASCE, **141**(6), 04014150.

Friedman, A., Phillips, B., Ahn, R., Chae, Y., Zhang, J., Cha, Y. and Sause, R. (2013), "RTHS (frame+damper)-3StoryPS-single MR damper (floor 1)", *Network for Earthquake Engineering Simulation (distributor), Dataset*, doi: 10, D3G15TB42.

Gao, X., Castaneda, N. and Dyke, S.J. (2013), "Real time hybrid simulation: from dynamic system, motion control to experimental error", *Earthq. Eng. Struct.*, **44**(6), 815-832.

Gao, X., Castaneda, N. and Dyke, S.J. (2014), "Experimental validation of a generalized procedure for MDOF real-time hybrid simulation", *J. Eng. Mech.*, ASCE, **140**(4), 04013006.

Guo, T., Chen, C., Xu, W.J. and Sanchez, F. (2014), "A frequency response analysis approach for quantitative assessment of actuator tracking for real-time hybrid simulation", *Smart. Struct.*, **23**(4), 045042.

Guo, T., Xu, W.J. and Chen, C. (2014), "Analysis of decimation techniques to improve computational efficiency of a frequency-domain evaluation approach for real-time hybrid simulation", *Smart. Struct. Syst.*, **14**(6), 1197-1220.

Horiuchi, T., Inoue, M., Konno, T. and Namita, Y. (1999), "Real-time hybrid experimental system with actuator delay compensation and its application to a piping system with energy absorber", *Earthq. Eng. Struct.*, **28**(10), 1121-1141.

Horiuchi, T. and Konno, T. (2001), "A new method for compensating actuator delay in real-time hybrid experiment", *Philos. T. Roy. Soc. A.*, **359**(1786), 1893-1909.

Karavasilis, T.L., Ricles, J.M., Sause, R. and Chen, C. (2011), "Experimental evaluation of the seismic performance of steel MRFs with compressed elastomer dampers using large-scale real-time hybrid simulation", *Eng. Struct.*, **33**(6), 1859-1869.

Kwon, O., Amr S. Elnashai and Billie F. Spencer (2008), "A framework for distributed analytical and hybrid simulations", *Struct. Eng. Mech.*, **30**(3), 331-350.

Mahin, S.A., Shing, P.B., Thewalt, C.R. and Hanson, R.D. (1989), "Pseudodynamic test method-current status and future direction", *J. Struct. Eng.*, ASCE, **115**(8), 2113-2128.

Mercan, O. and Ricles, J.M. (2007), "Stability and accuracy analysis of outer loop dynamics in real-time pseudodynamic

testing of SDOF systems", *Earthq. Eng. Struc.*, **36**(11), 1523-1543.

Mosqueda, G., Stojadinovic, B. and Mahin, S.A. (2007a), "Real-time error monitoring for hybrid simulation. Part I: methodology and experimental verification", *J. Struct. Eng.*, ASCE, **133**(8), 1100-1108.

Mosqueda, G., Stojadinovic, B. and Mahin, S.A. (2007b), "Real-time error monitoring for hybrid simulation. Part II: structural response modification due to errors", *J. Struct. Eng.*, ASCE, **133**(8), 1109-1117.

Nakashima, M., Kato, H. and Takaoka, E. (1992), "Development of real-time pseudodynamictesting", *Earthq. Eng. Struct.*, **21**(1), 79-92.

PEER Strong Ground Motion Database (2009), http://peer.berkeley.edu

Phillips, B.M. and Spencer, B.F. (2012), "Model-based multi actuator control for real-time hybrid simulation", *J. Struct. Eng.*, ASCE, **139**(2), 219-228.

Kwon, O., Elnashai, A.S. and Spencer, B.F. (2008), "A framework for distributed analytical and hybrid simulations", *Struct. Eng. Mech.*, **30**(3), 331-350.

Ricles, J.M. (2008), "Advanced servo-hydraulic control and real-time testing of damped structures", https://nees.org/warehouse/project/711.

Wallace, M.I., Sieber, J., Neild, S.A., Wagg, D.J. and Krauskopf, B. (2005), "Stability analysis of real-time dynamic substructuring using delay differential equation models", *Earthq. Eng. Struct.*, **34**(15), 1817-32.

Wen, Y.K. (1980), "Equivalent linearization for hysteretic systems under random excitation", *J. Appl. Mech. T.*, ASME, **47**(1), 150-154.

CC